

Quantum oscillations with topological phases in a kagome metal CsTi_3Bi_5

Yongkang Li, Hengxin Tan, and Binghai Yan*

Department of Condensed Matter Physics, Weizmann Institute of Science, Rehovot 7610001, Israel

(Dated: July 11, 2023)

Quantum oscillations can reveal Fermi surfaces and their topology in solids and provide a powerful tool for understanding transport and electronic properties. It is well established that the oscillation frequency maps the Fermi surface area by Onsager's relation. However, the topological phase accumulated along the quantum orbit remains difficult to estimate in calculations, because it includes multiple contributions from the Berry phase, orbital and spin moments, and also becomes gauge-sensitive for degenerate states. In this work, we develop a gauge-independent Wilson loop scheme to evaluate all topological phase contributions and apply it to CsTi_3Bi_5 , an emerging kagome metal. We find that the spin-orbit coupling dramatically alters the topological phase compared to the spinless case. Especially, oscillation phases of representative quantum orbits demonstrate a strong 3D signature despite their cylinder-like Fermi surface geometry. Our work reveals the Fermi surface topology of CsTi_3Bi_5 and paves the way for the theoretical investigation of quantum oscillations in realistic materials.

I. INTRODUCTION

Kagome lattice, a 2D corner-sharing triangle lattice, has attracted much interest due to its geometric frustration and non-trivial band geometry. Among various materials containing such 2D lattice structure, Kagome material family AV_3Sb_5 ($A = \text{K, Rb, Cs}$) [1] receives special attention since it exhibits many exotic quantum phenomena including \mathbb{Z}_2 topology and flat bands [2–4], possible unconventional superconductivity [2, 3, 5–9] and density wave order [2–8, 10–15]. However, because of the interplay and competition between different correlated states, the origin of these physical properties and their relation to the unique electronic structure remains elusive.

Recently, a new Ti-based Kagome material ATi_3Bi_5 ($A = \text{K, Rb, Cs}$) isostructural to AV_3Sb_5 is synthesized [16] and investigated [16–24]. Unlike V-based AV_3Sb_5 family, the charge density wave (CDW) order is absent in ATi_3Bi_5 family as shown in transport and scanning tunneling microscopy (STM) experiments [16, 17, 19, 22, 23, 25]. First-principles calculation also shows the absence of lattice structural instability [21]. Hence, ATi_3Bi_5 could serve as a complementary system to AV_3Sb_5 , in which the origin of these exotic phenomena and their relation to electronic properties can be investigated without reference to lattice's effect. For example, the observed two-fold rotational symmetry and orbital selectivity in the electronic structure of ATi_3Bi_5 [17, 19, 22, 25] may form a pure electronic nematic phase, similar to that in Fe-based high-temperature superconductors [26]. Understanding the band structure and Fermi surface of ATi_3Bi_5 is crucial for further investigating these correlating properties.

Quantum oscillation measurement is one way to measure the Fermi surface topology as well as its

associated properties like cyclotron mass and carrier mobility [27]. More importantly, the phase of the fundamental oscillation is related to the band topology. Usually, a π phase shift in the oscillation is regarded as π Berry phase which indicates a topological band structure [28–30]. The quantum oscillation analysis from this perspective has been carried out in AV_3Sb_5 [31–34] and also recently in ATi_3Bi_5 [16, 24], which claims nontrivial band topology due to this π Berry phase.

The topological phase actually has other contributions entangled with the Berry phase [35, 36]. Especially in the degenerate case with strong spin-orbit coupling (SOC), such π phase may mainly come from orbital or spin magnetic moment other than the Berry phase, as revealed recently in CsV_3Sb_5 [37]. Hence, the analysis of the topological properties based on the phase shift in quantum oscillation should consider all contributions. Apart from the experiment, this phase can be independently evaluated from ab-initio band structures. However, such calculation has to deal with the gauge fixing problem in the presence of degeneracy which is common for centrosymmetric nonmagnetic materials. A numerical study for all phase contributions without gauge ambiguities has not been explored in detail before.

In this work, we develop a Wilson loop method to determine the quantum oscillation phase and apply it to CsTi_3Bi_5 . We first detail the method which has explicit gauge independence and can be implemented conveniently in the case of degenerate bands. Then combining this method with first-principles calculation we resolve the Fermi surface of CsTi_3Bi_5 and determine the total oscillation phase for all quantum orbits. Its relation to the Fermi surface geometry and band topology is clarified at last. The 3D nature of several representative quantum orbits present is imprinted in the topological phase, although related Fermi surfaces show a cylinder-like shape. Our work provides a useful theoretical tool to investigate the Fermi surfaces and topological electronic properties in materials.

* binghai.yan@weizmann.ac.il

II. OVERVIEW ON THE QUANTUM OSCILLATION PHASE

In the presence of a strong magnetic field, the physical quantities (e.g., resistance and magnetization) show oscillation with respect to a magnetic field (B) due to the formation of quantized Landau levels (LLs). Under the semiclassical limit in which the scale of k -space orbit is much larger than the inverse of magnetic length l_B^{-1} ($l_B = \sqrt{\hbar/eB}$), the oscillation is periodic with respect to $1/B$ and can be expanded as a sum of Fourier series in general:

$$\delta A = \sum_i \sum_r A_{i,r} \cos [r(l_B^2 S_{F,i} + \theta_i + \phi_{M,i}) + \delta_i + \varphi_A]. \quad (1)$$

Here, A is the physical quantity being measured which is usually magnetization M or longitudinal resistivity ρ_{xx} , δA is the oscillation part and $A_{i,r}$ is the oscillation amplitude for the r -th harmonic of the i -th extremal orbit. $S_{F,i}$ is the momentum space area of the i -th extremal orbit on Fermi surface and determines the i -th oscillation frequency. Here the total oscillation phase is decomposed into four parts: θ_i is the first-order correction to the dynamical phase including the geometry phase and (orbital and spin) magnetic moment phase. $\phi_{M,i}$ is Maslov correction which equals to π for a simple closed orbit. δ_i is dimension related phase resulting from the integration over k_z if a 3D solid is measured (suppose B is along z direction). The last term φ_A is measured quantity (A) related phase (see the following discussion). All phases except φ_A depend only on the Fermi surface properties and are universal for any oscillatory quantity. Below we show that each phase can be determined from first-principles calculations to understand experiments. We note that a comprehensive theory on quantum oscillations was established in Refs. [35, 36]. We first overview this theory and then introduce the Wilson loop method to compute the topological phase.

A. Phase θ

The first two phases θ and ϕ_M (below we focus on a single orbit and ignore the subscript i) are related to LLs. In general, there are no simple rules to determine the exact LL for arbitrary band structure. However, in the semiclassical limit, approximate LL can be determined from Bohr-Sommerfeld-like quantization rules. For a group of D -fold degenerate bands, the j -th LLs can be obtained up to leading order in l_B^{-1} as,

$$l_B^2 S(E_{a,j}) + \lambda_a + \phi_M = 2\pi j + O(l_B^{-2/3}). \quad (2)$$

$a \in \mathbb{Z}_D := \{1, \dots, D\}$ is the band index among D degenerate bands and λ_a is a phase that we are interested. λ_a is equivalent to θ if there is no degeneracy, i.e., $D = 1$.

ϕ_M is Maslov correction and can be determined from the topology of the orbit, which equals π for a simple closed orbit.

Because of degeneracy, D LLs create D oscillation terms with the same frequency $F = \hbar S_F / 2\pi e$ by Onsager's relation but different phase shift λ_a . It amounts to a single oscillation term with reduced amplitude C and effective phase shift θ ,

$$\sum_{a=1}^D \cos [r(l_B^2 S_F + \lambda_a + \phi_M)] = C \cos [r(l_B^2 S_F + \theta + \phi_M)]. \quad (3)$$

For example, all bands are doubly degenerate ($D = 2$) in the presence of combined inversion and time reversal (\mathcal{PT}) symmetries, which is the case of kagome metals CsV₃Sb₅ and CsTi₃Bi₅. We regulate $\lambda_{1,2}$ in the range of $[-\pi, \pi]$ and then \mathcal{PT} symmetry leads to $\lambda_1 = -\lambda_2$. Hence, summing two cosine functions in Eq.(3) leads to

$$\theta = \begin{cases} 0, & \text{if } |\lambda_1| < \pi/2 \\ \pi, & \text{if } |\lambda_1| > \pi/2 \end{cases} \quad (4)$$

$$C = |\cos(\lambda_1)|,$$

One can find θ is a quantized topological invariant (0 or π) [35] insensitive to orbit details.

In general, phase λ_a can be determined from the spectrum $\{e^{i\lambda_a}\}_{a=1}^D$ of propagator [35, 36]

$$\mathcal{A}[\sigma] = \overline{\text{exp}} \left[i \oint_{\sigma} \{(\mathbf{A} + \mathbf{R}) \cdot d\mathbf{k} + Z(\sigma^z / v^\perp) dk\} \right]. \quad (5)$$

Here $\overline{\text{exp}}$ means path-ordered product, $\mathbf{A}(\mathbf{k})_{mn} = i \langle u_{m\mathbf{k}} | \nabla_{\mathbf{k}} u_{n\mathbf{k}} \rangle$ is non-Abelian Berry connection and

$$\begin{aligned} \mathbf{R}_{mn} \cdot d\mathbf{k} &= \sum_{l \notin \mathbb{Z}_D} A_{ml}^x \Pi_{ln}^y dk_x / 2v_y + (x \leftrightarrow y) \\ &= -i\hbar \sum_{l \notin \mathbb{Z}_D} \frac{\Pi_{ml}^x \Pi_{ln}^y}{\epsilon_{m\mathbf{k}} - \epsilon_{l\mathbf{k}}} \frac{dk_x}{2v_y} + (x \leftrightarrow y) \end{aligned} \quad (6)$$

$$= -(M_z / ev^\perp) dk, \quad (7)$$

is Roth term and represents the orbital correction ($-M_z B_z$) to the band energy. $\mathbf{\Pi}(\mathbf{k})_{ln} = \langle u_{l\mathbf{k}} | (1/\hbar) \nabla_{\mathbf{k}} \hat{H}(\mathbf{k}) | u_{n\mathbf{k}} \rangle$ is velocity matrix element and $\mathbf{v} = \mathbf{\Pi}_{nn}$ is group velocity. $\epsilon_{m\mathbf{k}}$ is band energy and v^\perp is the velocity in xy plane. $M_z = i(e\hbar/2) \sum_{l \notin \mathbb{Z}_D} \Pi_{ml}^x \Pi_{ln}^y / (\epsilon_{m\mathbf{k}} - \epsilon_{l\mathbf{k}}) - (x \leftrightarrow y)$ is the self rotation part of orbital magnetic moment [38]. Furthermore, $\sigma_{z,mn} = \langle u_{l\mathbf{k}} | \hat{\sigma}_z | u_{n\mathbf{k}} \rangle$ ($\hat{\sigma}_z$ is spin Pauli matrix) and $Z = g_0 \hbar / 4m$. The last term is the spin Zeeman term. Once the propagator ($\mathcal{A}[\sigma]$) is known, the phase λ_a can be easily obtained by diagonalizing it.

Though its formulation is clear in theory, the numerical calculation of this propagator needs to deal with the derivatives in the Berry connection. Besides, the multi-band magnetic moment (including orbital and spin) is a gauge covariant quantity whose matrix elements

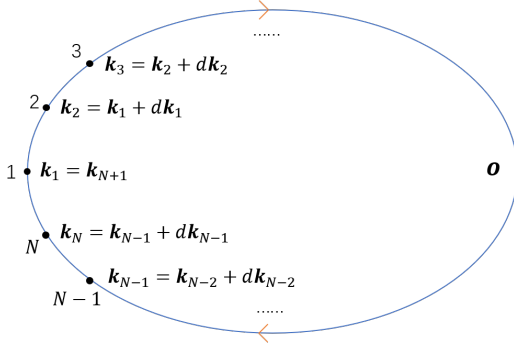


FIG. 1. The Wilson loop \circ for calculation of propagator \mathcal{A} . Here it's discretized to N points and the circulation direction is clockwise.

depend on the gauge. If a random gauge is chosen, the magnetic moment transforms independently at each point along the orbit, rendering the (5) meaningless. To deal with these problems, one can choose a smooth gauge by finding the maximally localized Wannier function[39]. Alternatively, the Wilson loop method[40–42] can be applied to avoid the choice of any specific gauge. Below, we shall use the Wilson loop method for the calculation of λ_a .

In this way, the quantum orbit is discretized into N segments (Fig.1) and the propagator is written as the product for each segment. If the segment is small enough, the exponent can be split into Berry connection and magnetic moment parts.

$$\begin{aligned} \mathcal{A}[\circ] &= \prod_{i=1}^N \exp \left\{ i \left[(\mathbf{A}(\mathbf{k}_i) + \mathbf{R}(\mathbf{k}_i)) \cdot d\mathbf{k}_i + Z \frac{\sigma_z}{v_{\perp}} |d\mathbf{k}_i| \right] \right\} \\ &\approx \prod_{i=1}^N \exp [i\mathbf{A}(\mathbf{k}_i) \cdot d\mathbf{k}_i] \exp \left[i\mathbf{R}(\mathbf{k}_i) \cdot d\mathbf{k}_i + iZ \frac{\sigma_z}{v_{\perp}} |d\mathbf{k}_i| \right]. \end{aligned} \quad (8)$$

For numerical calculation, the Berry connection part is usually expressed by an overlap matrix $M^i = \exp [i\mathbf{A}(\mathbf{k}_i) \cdot d\mathbf{k}_i]$. M_i is a D by D matrix with $M_{mn}^i = \langle u_{m\mathbf{k}_{i+1}} | u_{n\mathbf{k}_i} \rangle$.

The last ingredient for the propagator is an appropriate expression for the Roth term which shows explicit gauge covariance. It can be written as a summation of velocity matrix elements over *all* other states as in (6). Instead, we propose another method that considers only D degenerate states on the Fermi surface using the covariant derivative[43]. The covariant derivative is defined as

$$|D_{\alpha} u_{n\mathbf{k}}\rangle = Q_{\mathbf{k}} |\partial_{\alpha} u_{n\mathbf{k}}\rangle, \quad Q_{\mathbf{k}} := I - \sum_{a \in \mathbb{Z}_D} |u_{a\mathbf{k}}\rangle \langle u_{a\mathbf{k}}|. \quad (9)$$

In numerical calculation, it can be evaluated as an

appropriate finite difference[43]

$$|D_{\alpha} u_{n\mathbf{k}}\rangle = \frac{1}{2|q_{\alpha}|} (|\bar{u}_{n,\mathbf{k}+q_{\alpha}}\rangle - |\bar{u}_{n,\mathbf{k}-q_{\alpha}}\rangle), \quad (10)$$

where the dual state $|\bar{u}_{n,\mathbf{k}+q}\rangle$ is a linear combination of $|u_{n,\mathbf{k}+q}\rangle$ and has the property $\langle \bar{u}_{m\mathbf{k}} | \bar{u}_{n\mathbf{k}+q} \rangle = \delta_{mn}$. This ensures the orthogonality between the covariant derivative and states in degenerate space, i.e. $\langle u_{m\mathbf{k}} | D_{\alpha} u_{n\mathbf{k}} \rangle = 0$. Dual states are constructed as

$$|\bar{u}_{n,\mathbf{k}+q}\rangle = \sum_{n'} \left(S_{\mathbf{k},\mathbf{k}+q}^{-1} \right)_{n'n} |u_{n',\mathbf{k}+q}\rangle \quad (11)$$

and

$$(S_{\mathbf{k},\mathbf{k}+q})_{nn'} = \langle u_{n\mathbf{k}} | u_{n',\mathbf{k}+q} \rangle. \quad (12)$$

Using covariant derivative, Eq. (6) is expressed only by states inside the degenerate space

$$\begin{aligned} \mathbf{R}_{mn} \cdot d\mathbf{k} &= -\frac{i}{\hbar} \sum_{l \notin \mathbb{Z}_D} A_{ml}^x (\varepsilon_{n\mathbf{k}} - \varepsilon_{l\mathbf{k}}) A_{ln}^y dk_x / 2v_y + (x \leftrightarrow y) \\ &= -\frac{i}{\hbar} \sum_{l \notin \mathbb{Z}_D} \langle D_x u_{m\mathbf{k}} | u_{l\mathbf{k}} \rangle (\varepsilon_{n\mathbf{k}} - \varepsilon_{l\mathbf{k}}) \langle u_{l\mathbf{k}} | D_y u_{n\mathbf{k}} \rangle dk_x / 2v_y \\ &\quad + (x \leftrightarrow y) \\ &= -\frac{i}{\hbar} \left\langle D_x u_{m\mathbf{k}} | \varepsilon_{n\mathbf{k}} - \hat{H}(\mathbf{k}) | D_y u_{n\mathbf{k}} \right\rangle dk_x / 2v_y + (x \leftrightarrow y). \end{aligned} \quad (13)$$

In Appendix we show both Eq. (6) and Eq. (13) are gauge independent, which can be implemented easily in first-principles calculation. The Eq. (6) is practical for tight-binding models with a small number of bands but quite tedious if the total number of bands is large. The Eq. (13) avoids these problems and focuses only on the degenerate space and it is convenient when covariant derivatives can be easily calculated.

B. Phase δ

The above discussion about phase θ is for a single k -plane perpendicular to the magnetic field. For 3D material, one needs to integrate over k_z to get the contribution from the whole Fermi surface. Extremal orbits will dominate in the integration and this procedure will introduce another phase δ for each of them, which is generally $\pm\pi/4$ (+ for minimum cross-section and – for maximum cross-section). $\delta = 0$ for 2D material since there is only one k -plane. But for a nearly cylindrical Fermi surface (e.g., Fig.2(c)), δ lies between these two limits. Below we adopt a simple model from Refs. [27, 44] to determine δ for every extremal orbit that lies in a mirror plane. Here, we assume \mathcal{PT} symmetry for simplicity.

The oscillation of 3D Fermi surface is calculated first for a 2D plane with thickness dk_z and then integrate with respect to k_z , i.e.

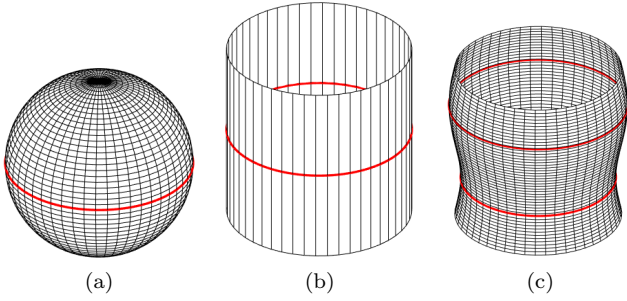


FIG. 2. (a) Spherical Fermi surface, (b) perfect cylindrical Fermi surface, and (c) nearly cylindrical Fermi surface. In both cases, the red circle shows the extremal orbit.

$$\begin{aligned}
 A_r &= \sum_a \int dk_z A_r(k_z) \cos \left[r(2\pi \frac{F(k_z)}{B} + \lambda_a(k_z)) + \phi_M \right] \\
 &\propto \int dk_z A_r(k_z) \cos \left[r(2\pi \frac{F(k_z)}{B} + \theta(k_z)) + \phi_M \right], \quad (14)
 \end{aligned}$$

$$\begin{aligned}
 A_r &\propto \text{Re} \int \exp \left[i(2\pi r \frac{F(k_z)}{B} + r\theta + \phi_M) \right] dk_z \\
 &\propto \text{Re} \exp \left[i(2\pi r \frac{F_0}{B} + r\theta + \phi_M) \right] \int \exp \left[\text{sgn}(F_2) i \frac{\pi}{2} x^2 (1 + \alpha x^2) \right] dx \\
 &\propto \cos \left[r(2\pi \frac{F_0}{B} + \theta) + \phi_M + \delta \right]. \quad (16)
 \end{aligned}$$

where phase δ is the argument of the last integral

$$\delta = \arg \left\{ \int_{x_m}^{x_m} \exp \left[\text{sgn}(F_2) i \frac{\pi}{2} x^2 (1 + \alpha x^2) \right] dx \right\}. \quad (17)$$

δ was numerically determined by carrying out the integral with given value α [27, 44], for which F_2, F_4 can be found from the polynomial fitting of $F(k_z)$ around the extremal orbit. The integral limit x_m can be taken as ∞ when $\alpha > 0$ because the main contribution comes from $x \approx 0$. However, this argument does not apply when $\alpha < 0$ due to the two extra artificial extrema. Since the real cross-section varies monotonically on either side of $x = 0$, x_m should be taken less than the turning point $1/\sqrt{2|\alpha|}$ to avoid these artificial extrema. In calculation, the argument of the integral goes to a steady value before the turning point, which should be assigned as δ . It's obvious that $\delta = 0$ from Eq. (14) when $F(k_z) = F_0$. For a general 3D material, if $\alpha \rightarrow 0$ (i.e., $F_4 \rightarrow 0$ and $F_2 k_z^2$ is the leading dispersion), one can get $\delta = \pm\pi/4$. Otherwise, δ may take a value between 0 and $\pm\pi/4$.

where $A_r(k_z)$ is the oscillation amplitude of 2D plane, which depends on k_z through cyclotron frequency $F(k_z)$ and cyclotron mass $m(k_z)$. The relative change of $F(k_z)$ and $m(k_z)$ in the interval where the integral is appreciable is usually small. Hence in the integration of Eq. (14), $A_r(k_z)$ can be treated approximately as a constant while $F(k_z)$ in the cosine function can't be treated as fixed because $F(k_z) \gg B$. Maslov phase ϕ_M remains constant as long as the orbit on the Fermi surface doesn't change its topology. Moreover, \mathcal{PT} symmetry cause the phase $\theta(k_z)$ quantized to 0 or π as in Eq. (4). So the k_z dependence of θ can also be ignored and only the k_z -variation of $F(k_z)$ needs to be considered.

We expand $F(k_z)$ near its extremal value to the fourth order and all odd orders are zero due to mirror symmetry.

$$F(k_z) = F_0 + \frac{1}{2} F_2 k_z^2 + \frac{1}{24} F_4 k_z^4. \quad (15)$$

Introducing dimensionless variable $x = (2r|F_2|/B)^{1/2} k_z$ and $\alpha = \text{sgn}(F_2) \frac{F_4 B}{24r|F_2|^2}$ then the integration can be calculated as

C. Phase φ_A

The last phase φ_A depends on the type of physical quantity A . When A is the density of states (DOS), this phase vanishes $\varphi_{DOS} = 0$. For other quantities, φ_A represents the connection between the oscillation of A and the oscillation of DOS. For example, $\varphi_M = \pi/2$ if A is sample magnetization, and $\varphi_\chi = \pi$ if A is magnetic susceptibility. In four terminal devices, the longitudinal conductivity σ_{xx} oscillates in phase with DOS hence $\varphi_\sigma = 0$. But since $\sigma_{xx} = \rho_{xx}/(\rho_{xx}^2 + \rho_{xy}^2)$, the resistivity ρ_{xx} can be in phase (if $\rho_{xx} \ll \rho_{xy}$) or out of phase (if $\rho_{xx} \gg \rho_{xy}$) with σ_{xx} , so $\varphi_\rho = 0$ if $\rho_{xx} \ll \rho_{xy}$ or $\varphi_\rho = \pi$ if $\rho_{xx} \gg \rho_{xy}$ [32, 45].

To summarize, all the phases in the oscillation term Eq. (1) have the following intuitive explanations. First, the magnetic-field-dependent term $l_B^2 S_F$ is given by the combination of the de Broglie phase (determined by the number of wavelengths in an orbit) and the Aharonov–Bohm phase. Then there is a phase λ_a associated with each orbit and each band coming from geometric effects and magnetic moment energy. λ_a of

degenerate bands for the same orbit will combine to give the phase θ . The reflection of the wave packet at turning points in the orbit causes phase ϕ_M . These phases are the total phase for a single orbit lying in the $kx - ky$ plane. For 3D materials, k_z integration needs to be carried out to incorporate the whole Fermi surface's contribution, which gives phase δ . At last, depending on what quantity A is measured, there will be another phase ϕ_A if the oscillation of A is not synchronized with the oscillation of DOS.

III. RESULTS AND DISCUSSIONS

The crystal structure of CsTi_3Bi_5 is fully relaxed within the Density Functional Theory (DFT) as implemented in the Vennia *ab-initio* Simulation Package [46, 47]. The cutoff energy for the plane-wave basis set is 300 eV. The force convergence criteria is 5 meV/Å. The electronic structure is calculated with the full-potential local-orbital minimum-basis code (FPLO) [48]. The default atomic basis sets are employed for the wave function expansion. The generalized gradient approximation parameterized by Perdew, Burke, and Ernzerhof (PBE) [49] is employed to mimic the exchange-correlation interaction between electrons throughout. The Brillouin zone is sampled by a k -mesh of $12 \times 12 \times 6$. The tight-binding Hamiltonian of CsTi_3Bi_5 is extracted via the maximally localized Wannier functions [39] as implemented in FPLO, which enforces all crystal symmetries. The Wannier basis set is composed of the Ti d and Bi p orbitals. The Fermi surface is calculated with the tight-binding Hamiltonian on a k -mesh of $300 \times 300 \times 100$.

We mention that the above Wilson loop method for the total oscillation phase shift has been successfully applied to the \mathcal{PT} symmetric kagome metal CsV_3Sb_5 [37], which predicted consistent results with experiments. In the following, we will apply the Wilson loop method to the recently discovered kagome superconductor CsTi_3Bi_5 [16] to further demonstrate the reliability of this method. We note here that the characterization of the dimensionality of the quantum orbit by the phase δ has not been discussed in our previous work on CsV_3Sb_5 .

The band structure of CsTi_3Bi_5 with spin-orbit coupling is plotted in Fig.3(a), which contains rich topological properties. Due to the \mathcal{PT} symmetry in CsTi_3Bi_5 , each band is doubly degenerate. Characteristic features of the kagome lattice, such as Dirac points at K/H points away from the Fermi level which are gapped by SOC, van Hove singularities at M/L, and flat bands along M-K/L-H lines [19, 20, 22], are shown. There are also type II Dirac crossings on the Γ -M and A-L lines, which form a Dirac nodal line [19, 20, 22] in the Γ -M-A plane. Besides, both the experiment and theory have shown that CsTi_3Bi_5 has topological Dirac surface states at the $\bar{\Gamma}$ point on the (001) surface [18–20, 22, 23].

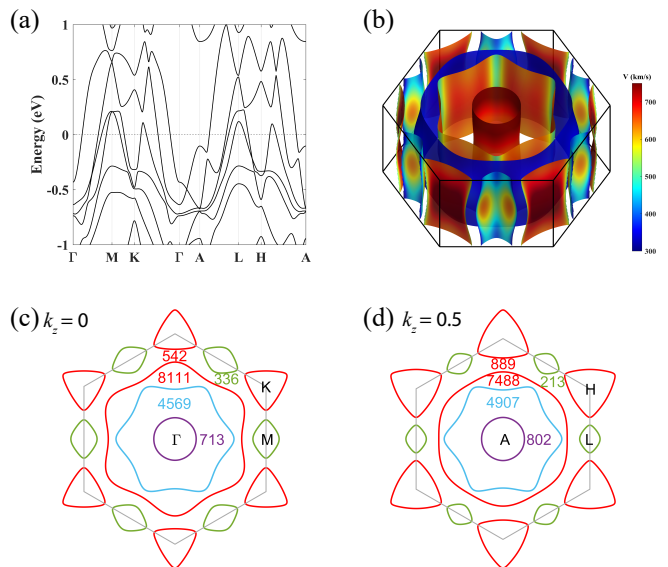


FIG. 3. (a) Band structure of CsTi_3Bi_5 with SOC. (b) 3D Fermi surface of CsTi_3Bi_5 , where the color representing the Fermi velocity is used to distinguish between different Fermi surfaces. (c) Fermi surfaces in $k_z = 0$ and (d) $k_z = 0.5$ (in units of $2\pi/c$, c is the lattice constant) mirror plane at the Fermi energy. The grey hexagon is the first Brillouin zone. Fermi surfaces with the same color come from the same band. The cyclotron frequencies (in units of T) are given.

The band structure on the $k_z = 0$ plane looks similar to the band structure on the $k_z = 0.5$ plane (in units of $2\pi/c$, c is the lattice constant), which indicates the quasi-two-dimensional feature of the electronic structure of CsTi_3Bi_5 . Indeed, the 3D Fermi surface shown in Fig.3(b) shows a good cylindrical shape for all pieces. There are totally four bands crossing the Fermi level creating five pieces of the Fermi surface. By sweeping k_z , all extremal quantum orbits perpendicular to the z -direction are found to locate at the two mirror planes $k_z = 0$ and $k_z = 0.5$, shown in Fig.3(c) and (d). The initial experiment reported an oscillation frequency of 200 T [16]. A more recent transport experiment [24] reported a series of oscillation frequencies, ranging from 217 to 1013 T. Our calculations show agreement with the experiments in the low-frequency region. For example, the calculated frequencies of 213, 336, and 542 T might correspond to the observed frequencies of 200/217, 281, 498 or 594 T, respectively. We notice that our calculated frequencies are slightly different from the calculations in Ref. 24, which might be induced by the mismatch of Fermi energy and/or different calculation parameters employed.

The cyclotron masses m^* of all calculated quantum orbits are summarized in Table I. Except for the two small pockets (336 and 213 T) around M/L points, all other orbits are electron pockets, whose cyclotron masses are defined as positive. The two largest hexagonal orbits centered around the Γ point (7488 and 8111 T) have

the largest cyclotron masses (1.6~1.7) while others have relatively small cyclotron masses.

The different quantum oscillation phases, as mentioned above, of all orbits are calculated and listed in Table I. Here every cyclotron orbit is a simple closed curve; thus the Maslov correction $\phi_M = \pi$ is omitted in the table. The phase λ_a is calculated by Eq. (13) with random gauge choices to test the gauge invariance, which presents the same results. We also confirm the relation $\lambda_1 = -\lambda_2$ for any two degenerate quantum orbits imposed by the \mathcal{PT} symmetry. Thus only the positive one λ_1 is listed. The Berry phases without (ϕ_{B0}) or with SOC (ϕ_B) are also listed for comparison. According to our previous discussion of Eq. (4), the final phase shift of the quantum orbit θ must be quantized to either 0 or π , depending on the magnitude of λ_1 , as listed in Table I. From these phases, it's clear that phase λ_1 is in general different from the Berry phase ϕ_B due to the orbital and spin magnetic moment contribution. Also for the \mathcal{PT} -symmetric system, the topology of the quantum orbit is not equivalent to the band topology of the individual Fermi surface. For example, the quantum orbits of 336 T (around M) and 8111 T (around Γ) have Berry phases ϕ_B close to 0 but the oscillation phase shifts are π . On the contrary, the quantum orbit of 4907 T (around A) has a Berry phase close to π but a zero oscillation phase shift. We note here that the strong SOC is important because these orbits have only a trivial Berry phase in the spinless case. Therefore, the incorporation of the magnetic moment contribution in the oscillation phase by SOC is crucial and the quantum phase shift extracted from the Landau fan diagram should be interpreted more carefully, rather than just interpreting it as the Berry phase. The recent experiment [24] finds that the quantum orbit of 281 T is non-trivial with a π phase shift ($\theta = \pi$), which is consistent with our calculated non-trivial quantum orbit of 336 T.

Because the 3D Fermi surface is nearly cylindrical, the dimension-related phase δ should be determined by considering higher order terms in the expansion of $F(k_z)$ in Eq. 15. From numerical calculations, the frequency F and cyclotron mass m^* of all extremal orbits have a small relative change on the Fermi surface (less than 5% in the interval $|\Delta k_z| \leq 0.1$). Since CsTi₃Bi₅ has \mathcal{PT} symmetry and all extremal orbits locate in mirror planes, Eq. (17) applies, which is used to calculate phase δ . The phase δ is calculated with the magnetic field B varying from 5 T to 40 T, covering the range of B in general oscillation experiments [31–33]. The variation of δ is very small in the considered B range. Thus the δ can be approximately treated as a constant, whose average value is listed in Table I. It shows that all quantum orbits except for the 213 and 802 T ones have a phase δ quite close to $\pm\pi/4$. Therefore, most orbits should be classified as 3D cases in quantum oscillation, even though the Fermi surfaces in Fig. 3(b) show a strong quasi-2D feature. On the other hand, the Fermi surface around A is almost dispersionless along k_z , so the δ for the quantum orbit of 802 T is closer

TABLE I. Extremal orbits of Fermi surfaces of CsTi₃Bi₅ at Fermi energy. Frequency (Freq.) is in units of T. k_z refers to the k_z plane (in units of $2\pi/c$, c is the lattice constant) where the corresponding extremal orbit is located in. The underlined frequency indicates a minimal Fermi surface cross-section and the others correspond to a maximal cross-section. The cyclotron mass m^* is in units of bare electron mass m_0 , where positive and negative values are for electron and hole pockets respectively. All orbits have Maslov correction $\phi_M = \pi$. ϕ_{B0} (ϕ_B) is Berry phase without (with) SOC and λ_1 is the phase of one of the band between two degenerate bands, defined in Eq. (5). δ is the phase related to the Fermi surface dimensionality. All phases are in units of π .

Freq. (T)	k_z ($2\pi/c$)	m^* (m_0)	ϕ_{B0} (π)	ϕ_B (π)	λ_1 (π)	θ (π)	δ (π)
<u>213</u>	0.5	-0.24	0	0.08	0.40	0	0.22
336	0	-0.22	0	0.16	0.59	1	-0.25
<u>542</u>	0	0.22	0	0.50	0.23	0	0.25
<u>713</u>	0	0.26	0	0.30	0.33	0	0.25
802	0.5	0.24	0	0.33	0.12	0	-0.14
889	0.5	0.32	1	0.26	0.10	0	-0.25
<u>4569</u>	0	0.72	0	0.74	0.42	0	0.25
4907	0.5	0.78	0	0.92	0.22	0	-0.25
<u>7488</u>	0.5	1.62	0	0.49	0.81	1	0.25
<u>8111</u>	0	1.68	0	0.38	0.82	1	-0.25

to zero than others. As a result, this quantum orbit is 2D. However, the quantum orbit of 713 T which comes from the same Fermi surface as the 802 T orbit but on the $k_z = 0$ plane, has a $\delta = \pi/4$. Consequently, the character (2D or 3D) of a quantum orbit should not be simply determined from the appearance of the related Fermi surface in the 3D k space.

IV. CONCLUSION

We theoretically studied the quantum oscillations by revealing their frequencies and topological phases through a Wilson loop method in CsTi₃Bi₅. We revealed three quantum orbits with $\theta = \pi$ phase shift. Despite most Fermi surfaces are quasi-2D, the dimension-related phase δ , beyond the angle-dependent frequency, clearly indicates their 3D nature. Our method can be applied to other quantum materials and provides a general way to study quantum oscillations assisted by first-principles calculations.

ACKNOWLEDGEMENT

B.Y. acknowledges the financial support by the European Research Council (ERC Consolidator Grant “NonlinearTopo”, No. 815869) and the ISF - Personal Research Grant (No. 2932/21).

APPENDIX

The most general gauge transformation is a $U(D)$ basis transformation among the degenerate bands

$$|u_{n\mathbf{k}}\rangle \rightarrow \sum_{m=1}^D U(\mathbf{k})_{mn} |u_{m\mathbf{k}}\rangle, \quad U^{-1} = U^\dagger, \quad (18)$$

It has already been shown that the propagator $\mathcal{A}[\mathbf{o}]$ is gauge covariant under such transformation[36] provided that the same wave function is used at the initial point and the final point, i.e. $|u(\mathbf{k}_{N+1})\rangle = |u(\mathbf{k}_1)\rangle$. Here we use the same way to show our numerical formula inherits this property so it's appropriate for calculation.

First, covariant derivatives transform as states under the $U(D)$ gauge transformation

$$\begin{aligned} |\bar{u}_{n,\mathbf{k}+\mathbf{q}}\rangle &\rightarrow \sum_{n'} (U(\mathbf{k})^\dagger S_{\mathbf{k},\mathbf{k}+\mathbf{q}} U(\mathbf{k}+\mathbf{q}))_{n'n}^{-1} |u_{n',\mathbf{k}+\mathbf{q}}\rangle \\ &= \sum_{n',m,l,m'} U(\mathbf{k}+\mathbf{q})_{n'm}^{-1} (S_{\mathbf{k},\mathbf{k}+\mathbf{q}}^{-1})_{ml} U(\mathbf{k})_{ln} \\ &\quad U(\mathbf{k}+\mathbf{q})_{m'n'} |u_{m',\mathbf{k}+\mathbf{q}}\rangle \\ &= \sum_{m,l} (S_{\mathbf{k},\mathbf{k}+\mathbf{q}}^{-1})_{ml} U(\mathbf{k})_{ln} |u_{m,\mathbf{k}+\mathbf{q}}\rangle \\ &= \sum_l U(\mathbf{k})_{ln} |\bar{u}_{l,\mathbf{k}+\mathbf{q}}\rangle \end{aligned} \quad (19)$$

which makes the covariant derivative expression of Roth term (13) transform covariantly. This is also true for the matrix elements expression of Roth term (6) and spin matrix σ_z , meaning that

$$\begin{aligned} \mathbf{R}(\mathbf{k}_i)_{mn} \cdot d\mathbf{k}_i &\rightarrow U(\mathbf{k}_i)^{-1} \mathbf{R}(\mathbf{k}_i)_{mn} \cdot d\mathbf{k}_i U(\mathbf{k}_i) \\ \sigma_z(\mathbf{k}_i)_{mn} \cdot d\mathbf{k}_i &\rightarrow U(\mathbf{k}_i)^{-1} \sigma_z(\mathbf{k}_i)_{mn} \cdot d\mathbf{k}_i U(\mathbf{k}_i) \end{aligned} \quad (20)$$

Therefore, the second term in (8) is also gauge covariant

$$\begin{aligned} &\exp \left[i\mathbf{R}(\mathbf{k}_i) \cdot d\mathbf{k}_i + iZ \frac{\sigma_z}{v_\perp} |d\mathbf{k}_i| \right] \\ &\rightarrow \exp \left\{ iU(\mathbf{k}_i)^{-1} \left[\mathbf{R}(\mathbf{k}_i) \cdot d\mathbf{k}_i + Z \frac{\sigma_z}{v_\perp} |d\mathbf{k}_i| \right] U(\mathbf{k}_i) \right\} \\ &= U(\mathbf{k}_i)^{-1} \exp \left[i\mathbf{R}(\mathbf{k}_i) \cdot d\mathbf{k}_i + iZ \frac{\sigma_z}{v_\perp} |d\mathbf{k}_i| \right] U(\mathbf{k}_i) \end{aligned} \quad (21)$$

Besides, the overlap matrix $M_{mn}^i = \langle u_{m\mathbf{k}_{i+1}} | u_{n\mathbf{k}_i} \rangle$ transforms like

$$M^i \rightarrow U(\mathbf{k}_{i+1})^{-1} M^i U(\mathbf{k}_i) \quad (22)$$

Hence, the covariance of discretized propagator (8) follows from the transformation properties of the two separate terms as

$$\begin{aligned} \mathcal{A}[\mathbf{o}] &\rightarrow \prod_{i=1}^N U(\mathbf{k}_{i+1})^{-1} M^i U(\mathbf{k}_i) \cdot U(\mathbf{k}_i)^{-1} \\ &\quad \exp \left[i\mathbf{R}(\mathbf{k}_i) \cdot d\mathbf{k}_i + iZ \frac{\sigma_z}{v_\perp} |d\mathbf{k}_i| \right] U(\mathbf{k}_i) \\ &= U(\mathbf{k}_{N+1})^{-1} \\ &\quad \left\{ \prod_{i=1}^N M^i \cdot \exp \left[i\mathbf{R}(\mathbf{k}_i) \cdot d\mathbf{k}_i + iZ \frac{\sigma_z}{v_\perp} |d\mathbf{k}_i| \right] \right\} U(\mathbf{k}_1) \\ &= U(\mathbf{k}_1)^{-1} \mathcal{A}[\mathbf{o}] U(\mathbf{k}_1) \end{aligned} \quad (23)$$

Since propagator $\mathcal{A}[\mathbf{o}]$ transforms covariantly, its spectrum $\{e^{i\lambda_a}\}_{a=1}^D$ is gauge invariant. In other words, the phase λ_a obtained through these numerical formulas is uniquely determined (module 2π) independent of gauge choice in the calculation.

-
- [1] Brenden R. Ortiz, LÍdia C. Gomes, Jennifer R. Morey, Michal Winiarski, Mitchell Bordelon, John S. Mangum, Iain W. H. Oswald, Jose A. Rodriguez-Rivera, James R. Neilson, Stephen D. Wilson, Elif Ertekin, Tyrel M. McQueen, and Eric S. Toberer, "New kagome prototype materials: discovery of KV_3Sb_5 , RbV_3Sb_5 , and CsV_3Sb_5 ," *Phys. Rev. Mater.* **3**, 094407 (2019).
- [2] Brenden R. Ortiz, Samuel M. L. Teicher, Yong Hu, Julia L. Zuo, Paul M. Sarte, Emily C. Schueller, A. M. Milinda Abeykoon, Matthew J. Krogstad, Stephan Rosenkranz, Raymond Osborn, Ram Seshadri, Leon Balents, Junfeng He, and Stephen D. Wilson, "CsV₃Sb₅: A \mathbb{Z}_2 Topological Kagome Metal with a Superconducting Ground State," *Phys. Rev. Lett.* **125**, 247002 (2020).
- [3] Brenden R. Ortiz, Paul M. Sarte, Eric M. Kenney, Michael J. Graf, Samuel M. L. Teicher, Ram Seshadri, and Stephen D. Wilson, "Superconductivity in the \mathbb{Z}_2 kagome metal KV_3Sb_5 ," *Phys. Rev. Mater.* **5**, 034801 (2021).
- [4] Yong Hu, Samuel M.L. Teicher, Brenden R. Ortiz, Yang Luo, Shuting Peng, Linwei Huai, Junzhang Ma, Nicholas C. Plumb, Stephen D. Wilson, Junfeng He, and Ming Shi, "Topological surface states and flat bands in the kagome superconductor CsV_3Sb_5 ," *Science Bulletin* **67**, 495–500 (2022).
- [5] Qiangwei Yin, Zhijun Tu, Chunsheng Gong, Yang Fu, Shaohua Yan, and Hechang Lei, "Superconductivity and Normal-State Properties of Kagome Metal RbV_3Sb_5 Single Crystals," *Chinese Physics Letters* **38**, 037403 (2021).
- [6] K. Y. Chen, N. N. Wang, Q. W. Yin, Y. H. Gu, K. Jiang, Z. J. Tu, C. S. Gong, Y. Uwatoko, J. P. Sun, H. C. Lei, J. P. Hu, and J.-G. Cheng, "Double Superconducting Dome and Triple Enhancement of T_c in the Kagome

- Superconductor CsV_3Sb_5 under High Pressure,” *Phys. Rev. Lett.* **126**, 247001 (2021).
- [7] Hui Chen, Haitao Yang, Bin Hu, Zhen Zhao, Jie Yuan, Yuqing Xing, Guojian Qian, Zihao Huang, Geng Li, Yuhan Ye, Sheng Ma, Shunli Ni, Hua Zhang, Qiangwei Yin, Chunsheng Gong, Zhijun Tu, Hechang Lei, Hengxin Tan, Sen Zhou, Chengmin Shen, Xiaoli Dong, Binghai Yan, Ziqiang Wang, and Hong-Jun Gao, “Roton pair density wave in a strong-coupling kagome superconductor,” *Nature* **599**, 222–228 (2021).
- [8] Hengxin Tan, Yizhou Liu, Ziqiang Wang, and Binghai Yan, “Charge density waves and electronic properties of superconducting kagome metals,” *Phys. Rev. Lett.* **127**, 046401 (2021).
- [9] Han-Shu Xu, Ya-Jun Yan, Ruotong Yin, Wei Xia, Shijie Fang, Ziyuan Chen, Yuanji Li, Wenqi Yang, Yanfeng Guo, and Dong-Lai Feng, “Multiband Superconductivity with Sign-Preserving Order Parameter in Kagome Superconductor CsV_3Sb_5 ,” *Phys. Rev. Lett.* **127**, 187004 (2021).
- [10] Yu-Xiao Jiang, Jia-Xin Yin, M. Michael Denner, Nana Shumiya, Brenden R. Ortiz, Gang Xu, Zurab Guguchia, Junyi He, Md Shafayat Hossain, Xiaoxiong Liu, Jacob Ruff, Linus Kautzsch, Songtian S. Zhang, Guoqing Chang, Ilya Belopolski, Qi Zhang, Tyler A. Cochran, Daniel Multer, Maksim Litskevich, Zi-Jia Cheng, Xian P. Yang, Ziqiang Wang, Ronny Thomale, Titus Neupert, Stephen D. Wilson, and M. Zahid Hasan, “Unconventional chiral charge order in kagome superconductor KV_3Sb_5 ,” *Nature Materials* **20**, 1353–1357 (2021).
- [11] Zuowei Liang, Xingyuan Hou, Fan Zhang, Wanru Ma, Ping Wu, Zongyuan Zhang, Fanghang Yu, J.-J. Ying, Kun Jiang, Lei Shan, Zhenyu Wang, and X.-H. Chen, “Three-Dimensional Charge Density Wave and Surface-Dependent Vortex-Core States in a Kagome Superconductor CsV_3Sb_5 ,” *Phys. Rev. X* **11**, 031026 (2021).
- [12] He Zhao, Hong Li, Brenden R. Ortiz, Samuel M. L. Teicher, Takamori Park, Mengxing Ye, Ziqiang Wang, Leon Balents, Stephen D. Wilson, and Ilija Zeljkovic, “Cascade of correlated electron states in the kagome superconductor CsV_3Sb_5 ,” *Nature* **599**, 216–221 (2021).
- [13] Takamori Park, Mengxing Ye, and Leon Balents, “Electronic instabilities of kagome metals: Saddle points and Landau theory,” *Phys. Rev. B* **104**, 035142 (2021).
- [14] Linpeng Nie, Kuanglv Sun, Wanru Ma, Dianwu Song, Lixuan Zheng, Zuowei Liang, Ping Wu, Fanghang Yu, Jian Li, Min Shan, Dan Zhao, Shunjiao Li, Baolei Kang, Zhimian Wu, Yanbing Zhou, Kai Liu, Ziji Xiang, Jianjun Ying, Zhenyu Wang, Tao Wu, and Xianhui Chen, “Charge-density-wave-driven electronic nematicity in a kagome superconductor,” *Nature* **604**, 59–64 (2022).
- [15] Hong Li, He Zhao, Brenden R. Ortiz, Yuzki Oey, Ziqiang Wang, Stephen D. Wilson, and Ilija Zeljkovic, “Unidirectional coherent quasiparticles in the high-temperature rotational symmetry broken phase of AV_3Sb_5 kagome superconductors,” **19**, 637–643 (2023).
- [16] Dominik Werhahn, Brenden R. Ortiz, Aurland K. Hay, Stephen D. Wilson, Ram Seshadri, and Dirk Johrendt, “The kagomé metals RbTi_3Bi_5 and CsV_3Sb_5 ,” *Zeitschrift für Naturforschung B* **77**, 757–764 (2022).
- [17] Hong Li, Siyu Cheng, Brenden R. Ortiz, Hengxin Tan, Dominik Werhahn, Keyu Zeng, Dirk Johrendt, Binghai Yan, Ziqiang Wang, Stephen D. Wilson, and Ilija Zeljkovic, “Electronic nematicity in the absence of charge density waves in a new titanium-based kagome metal,” (2022), [arXiv:2211.16477](https://arxiv.org/abs/2211.16477) [cond-mat.str-el].
- [18] Haitao Yang, Zhen Zhao, Xin-Wei Yi, Jiali Liu, Jing-Yang You, Yuhang Zhang, Hui Guo, Xiao Lin, Chengmin Shen, Hui Chen, Xiaoli Dong, Gang Su, and Hong-Jun Gao, “Titanium-based kagome superconductor CsTi_3Bi_5 and topological states,” (2022), [arXiv:2209.03840](https://arxiv.org/abs/2209.03840) [cond-mat.supr-con].
- [19] Yong Hu, Congcong Le, Zhen Zhao, Junzhang Ma, Nicholas C. Plumb, Milan Radovic, Andreas P. Schnyder, Xianxin Wu, Hui Chen, Xiaoli Dong, Jiangping Hu, Haitao Yang, Hong-Jun Gao, and Ming Shi, “Non-trivial band topology and orbital-selective electronic nematicity in a new titanium-based kagome superconductor,” (2022), [arXiv:2212.07958](https://arxiv.org/abs/2212.07958) [cond-mat.supr-con].
- [20] Jianguang Yang, Yuyang Xie, Zhen Zhao, Xinwei Yi, Taimin Miao, Hailan Luo, Hao Chen, Bo Liang, Wenpei Zhu, Yuhan Ye, Jing-Yang You, Bo Gu, Shenjin Zhang, Fengfeng Zhang, Feng Yang, Zhimin Wang, Qinjun Peng, Hanqing Mao, Guodong Liu, Zuyan Xu, Hui Chen, Haitao Yang, Gang Su, Hongjun Gao, Lin Zhao, and X. J. Zhou, “Observation of Flat Band, Dirac Nodal Lines and Topological Surface States in Kagome Superconductor CsTi_3Bi_5 ,” (2022), [arXiv:2212.04447](https://arxiv.org/abs/2212.04447) [cond-mat.supr-con].
- [21] Bo Liu, Minquan Kuang, Yang Luo, Yongkai Li, Linwei Huai, Shuting Peng, Zhiyuan Wei, Jianchang Shen, Bingqian Wang, Yu Miao, Xiupeng Sun, Zhipeng Ou, Yugui Yao, Zhiwei Wang, and Junfeng He, “Tunable van Hove singularity without structural instability in Kagome metal CsTi_3Bi_5 ,” (2022), [arXiv:2212.04460](https://arxiv.org/abs/2212.04460) [cond-mat.str-el].
- [22] Zhicheng Jiang, Zhengtai Liu, Haiyang Ma, Wei Xia, Zhonghao Liu, Jishan Liu, Soohyun Cho, Yichen Yang, Jianyang Ding, Jiayu Liu, Zhe Huang, Yuxi Qiao, Jiajia Shen, Wenchuan Jing, Xiangqi Liu, Jianpeng Liu, Yanfeng Guo, and Dawei Shen, “Flat bands, non-trivial band topology and electronic nematicity in layered kagome-lattice RbTi_3Bi_5 ,” (2022), [arXiv:2212.02399](https://arxiv.org/abs/2212.02399) [cond-mat.str-el].
- [23] Ying Zhou, Long Chen, Xuecong Ji, Chen Liu, Ke Liao, Zhongnan Guo, Jia’ou Wang, Hongming Weng, and Gang Wang, “Physical properties, electronic structure, and strain-tuned monolayer of the weak topological insulator RbTi_3Bi_5 with Kagome lattice,” (2023), [arXiv:2301.01633](https://arxiv.org/abs/2301.01633) [cond-mat.supr-con].
- [24] Xiaoli Dong, Yuhang Zhang, Xinwei Yi, Zhen Zhao, Jiali Liu, Ziyi Liu, Aini Xu, Dong Li, Zouyouwei Lu, Sheng Ma, Yue Liu, Jihu Lu, Hua Zhang, Hui Chen, Shiliang Li, Jinguang Cheng, Gang Su, Haitao Yang, Hong-Jun Gao, and Zhongxian Zhao, “de Haas-van Alphen oscillation reveals nontrivial Fermi surface topology in Kagome superconductor CsTi_3Bi_5 ,” *Research Square* (2023).
- [25] Haitao Yang, Yuhan Ye, Zhen Zhao, Jiali Liu, Xin-Wei Yi, Yuhang Zhang, Jinan Shi, Jing-Yang You, Zihao Huang, Bingjie Wang, Jing Wang, Hui Guo, Xiao Lin, Chengmin Shen, Wu Zhou, Hui Chen, Xiaoli Dong, Gang Su, Ziqiang Wang, and Hong-Jun Gao, “Superconductivity and orbital-selective nematic order in a new titanium-based kagome metal CsTi_3Bi_5 ,” (2022), [arXiv:2211.12264](https://arxiv.org/abs/2211.12264) [cond-mat.supr-con].
- [26] T.-M. Chuang, M. P. Allan, Jinho Lee, Yang Xie,

- Ni Ni, S. L. Bud'ko, G. S. Boebinger, P. C. Canfield, and J. C. Davis, "Nematic Electronic Structure in the "Parent" State of the Iron-Based Superconductor $\text{Ca}(\text{Fe}_{1-x}\text{Co}_x)_2\text{As}_2$," *Science* **327**, 181–184 (2010).
- [27] D. Shoenberg, *Magnetic Oscillations in Metals*, Cambridge Monographs on Physics (Cambridge University Press, 1984).
- [28] G. P. Mikitik and Yu. V. Sharlai, "Manifestation of berry's phase in metal physics," *Phys. Rev. Lett.* **82**, 2147–2150 (1999).
- [29] Igor A. Luk'yanchuk and Yakov Kopelevich, "Phase analysis of quantum oscillations in graphite," *Phys. Rev. Lett.* **93**, 166402 (2004).
- [30] Yuanbo Zhang, Yan-Wen Tan, Horst L. Stormer, and Philip Kim, "Experimental observation of the quantum hall effect and berry's phase in graphene," *Nature* **438**, 201–204 (2005).
- [31] K. Shrestha, R. Chapai, Bal K. Pokharel, D. Miertschin, T. Nguyen, X. Zhou, D. Y. Chung, M. G. Kanatzidis, J. F. Mitchell, U. Welp, Dragana Popović, D. E. Graf, B. Lorenz, and W. K. Kwok, "Nontrivial Fermi surface topology of the kagome superconductor CsV_3Sb_5 probed by de Haas–van Alphen oscillations," *Phys. Rev. B* **105**, 024508 (2022).
- [32] Yang Fu, Ningning Zhao, Zheng Chen, Qiangwei Yin, Zhijun Tu, Chunsheng Gong, Chuanying Xi, Xiangde Zhu, Yuping Sun, Kai Liu, and Hechang Lei, "Quantum Transport Evidence of Topological Band Structures of Kagome Superconductor CsV_3Sb_5 ," *Phys. Rev. Lett.* **127**, 207002 (2021).
- [33] Christopher Broyles, David Graf, Haitao Yang, Xiaoli Dong, Hongjun Gao, and Sheng Ran, "Effect of the Interlayer Ordering on the Fermi Surface of Kagome Superconductor CsV_3Sb_5 Revealed by Quantum Oscillations," *Phys. Rev. Lett.* **129**, 157001 (2022).
- [34] Ramakanta Chapai, Maxime Leroux, Vincent Oliviero, David Vignolles, Nicolas Bruyant, M. P. Smylie, D. Y. Chung, M. G. Kanatzidis, W.-K. Kwok, J. F. Mitchell, and Ulrich Welp, "Magnetic Breakdown and Topology in the Kagome Superconductor CsV_3Sb_5 under High Magnetic Field," *Phys. Rev. Lett.* **130**, 126401 (2023).
- [35] A. Alexandradinata, Chong Wang, Wenhui Duan, and Leonid Glazman, "Revealing the topology of fermi-surface wave functions from magnetic quantum oscillations," *Phys. Rev. X* **8**, 011027 (2018).
- [36] A. Alexandradinata and Leonid Glazman, "Semiclassical theory of landau levels and magnetic breakdown in topological metals," *Phys. Rev. B* **97**, 144422 (2018).
- [37] Hengxin Tan, Yongkang Li, Yizhou Liu, Daniel Kaplan, Ziqiang Wang, and Binghai Yan, "Emergent topological quantum orbits in the charge density wave phase of kagome metal CsV_3Sb_5 ," *arXiv:2303.04924* (2023).
- [38] Di Xiao, Ming-Che Chang, and Qian Niu, "Berry phase effects on electronic properties," *Rev. Mod. Phys.* **82**, 1959–2007 (2010).
- [39] Nicola Marzari and David Vanderbilt, "Maximally localized generalized wannier functions for composite energy bands," *Phys. Rev. B* **56**, 12847–12865 (1997).
- [40] Takahiro Fukui, Yasuhiro Hatsugai, and Hiroshi Suzuki, "Chern numbers in discretized brillouin zone: Efficient method of computing (spin) hall conductances," *Journal of the Physical Society of Japan* **74**, 1674–1677 (2005).
- [41] Rui Yu, Xiao Liang Qi, Andrei Bernevig, Zhong Fang, and Xi Dai, "Equivalent expression of \mathbb{Z}_2 topological invariant for band insulators using the non-Abelian Berry connection," *Phys. Rev. B* **84**, 075119 (2011).
- [42] Alexey A. Soluyanov and David Vanderbilt, "Wannier representation of \mathbb{Z}_2 topological insulators," *Phys. Rev. B* **83**, 035108 (2011).
- [43] Davide Ceresoli, T. Thonhauser, David Vanderbilt, and R. Resta, "Orbital magnetization in crystalline solids: Multi-band insulators, chern insulators, and metals," *Phys. Rev. B* **74**, 024408 (2006).
- [44] David Shoenberg and Ian M. Templeton, "Anomalous amplitudes and phases in the de haas-van alphen effect," *Physica D: Nonlinear Phenomena* **69**, 293–307 (1973).
- [45] Fei-Xiang Xiang, Xiao-Lin Wang, Menno Veldhorst, Shi-Xue Dou, and Michael S. Fuhrer, "Observation of topological transition of fermi surface from a spindle torus to a torus in bulk rashba spin-split bitecl," *Phys. Rev. B* **92**, 035123 (2015).
- [46] G. Kresse and J. Furthmüller, "Efficient iterative schemes for ab initio total-energy calculations using a plane-wave basis set," *Phys. Rev. B* **54**, 11169 (1996).
- [47] Georg Kresse and Jürgen Furthmüller, "Efficiency of ab-initio total energy calculations for metals and semiconductors using a plane-wave basis set," *Comput. Mater. Sci.* **6**, 15–50 (1996).
- [48] Klaus Koepnik and Helmut Eschrig, "Full-potential nonorthogonal local-orbital minimum-basis band-structure scheme," *Phys. Rev. B* **59**, 1743–1757 (1999).
- [49] John P. Perdew, Kieron Burke, and Matthias Ernzerhof, "Generalized gradient approximation made simple," *Phys. Rev. Lett.* **77**, 3865 (1996).